ChemComm

COMMUNICATION

View Article Online
View Journal | View Issue

Cite this: *Chem. Commun.*, 2025, **61**, 3848

Received 12th October 2024,
Accepted 3rd February 2025

DOI: 10.1039/d4cc05402d

rsc.li/chemcomm

An extended π-conjugated bipolar polymer cathode for rechargeable magnesium batteries: high capacity contributed by n- and p-doping and charge delocalization†

Shuai Cui,[a] Zhen Qin,[a] Hongda Gui,[b] Ting Li, *[a] Daohong Zhang *[a] and Fei Xu *[b]

An extended conjugated bipolar cathode material is developed for rechargeable Mg batteries, which undergoes p- and n-doping with charge delocalized to the large conjugated structures. The extended conjugated structure guarantees large charge density change and structure stability, leading to high capacity and good cycling stability.

With the rapid development of portable electronic devices and electric vehicles, it is urgent to develop high-performance, low-cost and environmentally friendly electrochemical energy-storage systems. Due to the abundant mineral resources, exploration of non-Li-ion batteries such as Na-, K-, Al- and Mg-ion batteries has gradually attracted the attention of researchers. Among them, rechargeable Mg batteries (RMBs) draw special interest because of the prominent advantages of the Mg metal anode, including high theoretical volume capacity (3833 mA h cm^{-3}), low reduction potential (−2.37 V *vs.* SHE), and low tendency to form dendrites during deposition.[1–6] These properties make RMBs a potential post-Li-ion battery energy-storage technology with great application potential.

Currently, the development of cathode materials is the main difficulty of RMBs. The high polarity of Mg^{2+} makes it hardly able to intercalate into the inorganic crystal lattice, and most reported inorganic cathodes show low capacities and inferior kinetic performances.[7–9] In contrast, organic conjugated polymers are promising cathode materials for RMBs because of the amorphous structures, delocalized negative charge and diverse designabilities.[10–12] The negative charge delocalization weakens the interaction with the Mg^{2+} cations, the amorphous structures favor the solid-phase Mg^{2+} diffusion, and the wide designability provides abundant structure selections. In particular, organic polymers with large conjugated structures are more favorable since they can more effectively alleviate the charge density change caused by Mg-association.[13–15] Considering the structure feature of large conjugated polymers, they could be designed as bipolar cathodes for RMBs with high specific capacities *via* full utilization of the charge density change during p- and n-doping. Therefore, in the present study, a large conjugated polymer is constructed by a combination of perylenetetracarboxylic diimide (PTCDI) and triphenylamine (tBA) units, which act as n- and p-doping groups, respectively (**PI-P-tBA**, Fig. 1a). Moreover, the covalent bonds between PTCDI and tBA groups guarantee conjugation of the perylene and benzene units, hence improving structure stability and specific capacity. Also, the inner space built by the polymer provides space for solid-state Mg^{2+} diffusion to improve the reaction kinetics.

PI-P-tBA was synthesized by a one-step imidization reaction (Fig. S1, ESI†) of perylenetetracarboxylic dianhydride (PTCDA) and tris(4-aminophenyl)amine (TAPA) according to a molar ratio of 3 : 2 (dianhydride and amino groups of 1 : 1).[16] The structures of tBA (p-type), PTCDI (n-type) and **PI-P-tBA** are shown in Fig. 1a. XRD (Fig. 1c), FT-IR (Fig. 1d) and Raman (Fig. 1e) were carried out to confirm the success of synthesis. As shown in the XRD patterns (Fig. 1c), the reactants of PTCDA and TAPA show obvious crystal characteristics, while **PI-P-tBA** is amorphous, demonstrating the occurrence of the reaction. FT-IR spectra (Fig. 1d) reveal the active groups of **PI-P-tBA** and the reactants, including the amino and carbonyl groups. The peaks of amino groups ($-NH_2$) of TAPA at 3400 and 3336 cm^{-1} completely disappear in **PI-P-tBA**, demonstrating the imidization. Meanwhile, two peaks ascribed to C–N bonds appear in **PI-P-tBA** at 1360 and 1330 cm^{-1}, which are attributed to the bonding with the PTCDI and tBA units, respectively. The original C–N bond in TAPA is located at 1329 cm^{-1}. Moreover, the peaks of carbonyl (C=O) also show an obvious shift to low frequencies from 1680–1800 cm^{-1} in

[a] *Key Laboratory of Catalysis and Energy Materials Chemistry of Ministry of Education & Hubei Key Laboratory of Catalysis and Materials Science, Hubei R&D Center of Hyperbranched Polymers Synthesis and Applications, South-Central Minzu University, Wuhan 430074, China. E-mail: liting@mail.scuec.edu.cn, daohong.zhang@scuec.edu.cn*

[b] *Key Laboratory of Hydraulic Machinery Transients, Ministry of Education, School of Power and Mechanical Engineering, Wuhan University, Wuhan 430072, China. E-mail: xufei2058@whu.edu.cn*

† Electronic supplementary information (ESI) available. See DOI: https://doi.org/10.1039/d4cc05402d

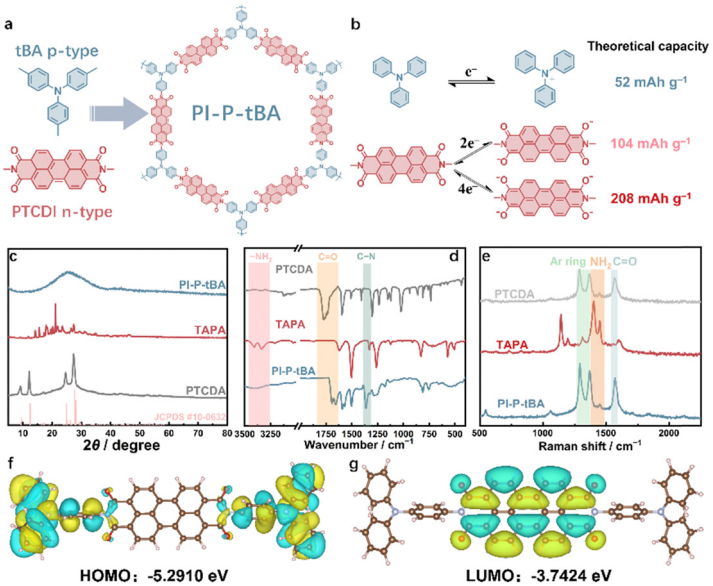

Fig. 1 (a) Structures of tBA, PTCDI and **PI-P-tBA**, (b) theoretical capacities of tBA and PTCDI in **PI-P-tBA** (calculation details in Fig. S2, ESI†), (c) XRD patterns, (d) FT-IR and (e) Raman spectra of TAPA, PTCDA and **PI-P-tBA**, and (f) HOMO and (g) LUMO of PTCDI with two tBA units.

PTCDA to 1600–1700 cm^{-1} in **PI-P-tBA**,[17,18] which is a characteristic feature of synthetic polyimides. The changes of amino and carbonyl groups are also reflected in the Raman spectra (Fig. 1e). The peaks of conjugated structure, amino and carbonyl groups are at 1260–1380, 1380–1460 and 1540–1600 cm^{-1}, respectively. The above results fully demonstrate the successful synthesis of **PI-P-tBA**. A repeating unit of **PI-P-tBA** (PTCDI with two tBA units) was selected to calculate the HOMO and LUMO (Fig. 1f and g). It is observed that the HOMO is mainly distributed at the two tBA units, indicating that they are introduced as p-doping groups. The LUMO is mainly distributed at the PTCDI units.

The electrochemical performances of **PI-P-tBA** were comparatively investigated within voltage ranges of 0.2–2.8 V and 0.2–3.2 V at 50 mA g^{-1} to illustrate the n- and p-doping

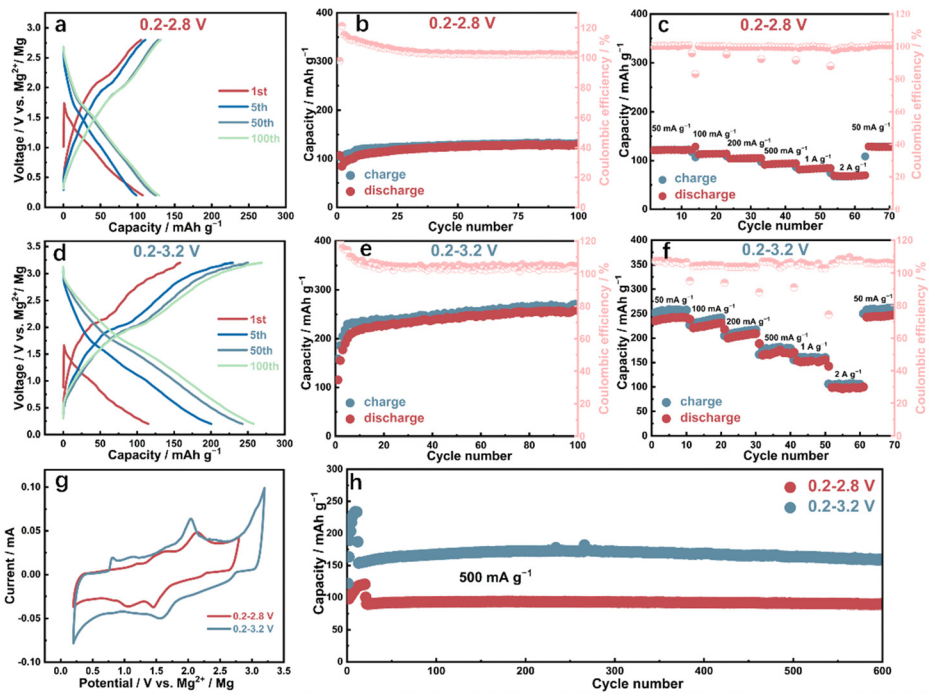

Fig. 2 (a) Charge/discharge profiles (50 mA g^{-1}), (b) cycling performance (50 mA g^{-1}) and (c) rate performance of **PI-P-tBA** with 0.2–2.8 V. (d) Charge/discharge profiles (50 mA g^{-1}), (e) cycling performance (50 mA g^{-1}) and (f) rate performance of **PI-P-tBA** with 0.2–3.2 V. (g) CV profiles of **PI-P-tBA** at 0.1 mV s^{-1} with the potential ranges of 0.2–2.8 and 0.2–3.2 V. (h) Long-term cycling of **PI-P-tBA** (first at 50 mA g^{-1} and then at 500 mA g^{-1}).

properties. As shown in Fig. 2a and b, **PI-P-tBA** shows a reversible capacity of 105 mA h g^{-1} within 0.2–2.8 V, which is in accordance with the two-electron enolization capacity of the PTCDI units (104 mA h g^{-1}, Fig. 1b). Although large conjugated PTCDI-based polyimides were proved in previous work indicating that enolization beyond two-electron can be achieved,[10] the introduction of an electron donor group (tBA) reduces the electron-accepting ability of **PI-P-tBA**, and thus resulting in a decrease in n-doping capacity. After 10 cycles of activation, the maximum capacity is reached and maintained, and the polarization decreases with cycling. The reversible capacities of **PI-P-tBA** increase significantly from 105 to 250 mA h g^{-1} upon the increase of the upper voltage from 2.8 to 3.2 V (Fig. 2d and e), corresponding to about a five-electron redox of **PI-P-tBA** (Fig. 1b, theoretical five-electron capacity of 260 mA h g^{-1}). Besides the one-electron p-doping capacity of the tBA unit (50 mA h g^{-1}), and the n-doping (enolization) of PTCDI is also improved (from 105 to 200 mA h g^{-1}) by increase of the upper voltage from 2.8 to 3.2 V, which also demonstrates the advantages of a large conjugated structure in high capacity *via* charge delocalization. The coulombic efficiency is higher than 100% for 0.2–3.2 V, suggesting that there might be slight dissolution of the discharged electrode materials. It is seen in Fig. 2e that **PI-P-tBA** maintains excellent cycling stability after the voltage range was widened to 0.2–3.2 V, which demonstrates the advantages of large conjugated polymers in the enhanced charge density change and improved structure stability during redox reactions. As shown in Fig. 2f, **PI-P-tBA** exhibits excellent rate performance within 0.2–3.2 V, delivering 243, 230, 205, 169 and 152 mA h g^{-1}, respectively, at 50, 100, 200, 500, 1000 and 2000 mA g^{-1} (charge and discharge curves shown in Fig. S6, ESI†).

To better compare the electrochemical performance differences with different potential ranges, cyclic voltammetry (CV) tests of 0.2–2.8 V and 0.2–3.2 V were performed for **PI-P-tBA**. Fig. 2g compares the CV curves after the activation. It is observed that the peak intensities are much higher with 0.2–3.2 V, indicating the enhanced redox activity of **PI-P-tBA** upon widening of the potential range. Significantly, such an enhancement is not only because of the p-doing within 2.8–3.2 V. But also, the n-doping within 0.2–2.8 V is also improved, reflected as increased current densities from 0.2–2.8 V. Moreover, the potential differences between the redox peaks decrease when the voltage range changes from 0.2–2.8 V to 0.2–3.2 V, indicating lower polarization and better reaction reversibility. Fig. S7c (ESI†) shows the CV comparison of the first few cycles and after activation with 0.2–3.2 V. It is clearly observed that the current densities are similar to those within 0.2–2.8 V during the initial cycles, while largely enhanced after the activation. Fig. 2h shows that high cycling stabilities are achieved for **PI-P-tBA** in both voltage ranges, providing 600-cycle capacity retention rates of 96% and 91%, respectively, for 0.2–2.8 V and 0.2–3.2 V.

To unveil the reaction mechanism of **PI-P-tBA**, the cathodes at charged and discharged states with different voltage ranges were characterized by FT-IR (Fig. 3a). It is observed that the C=O peaks (1740–1600 cm^{-1}) at the discharged state shift slightly towards the low frequency region compared with those in the charged state, which is a typical feature of C=O enolization and association with Mg^{2+} cations. More importantly, the stretching vibration of C–N bonds of two chemical states is observed at 1300–1400 cm^{-1}. The peak at 1360 cm^{-1} corresponds to the C–N bond of the PTCDI unit, whose peak intensity is weakened in the discharged state. This is attributed to the electron cloud density changes at discharge, during which the electron is delocalized to the conjugated structure, resulting in a more uniform distribution of electrons and hence a decrease of dipole moment of the C–N bond. Moreover, it is apparent that the peak intensity change is more obvious when cycled with 0.2–3.2 V than with 0.2–2.8 V, indicating that the overall conjugation degree is significantly improved and the charge delocalization is enhanced upon increasing the upper voltage. In contrast, for the C–N bond corresponding to the tBA unit at 1330 cm^{-1}, the peak intensity decreases in the charge state. This is because the tBA unit is an electron donor and loses electrons during the charge process, resulting in a decreasing dipole moment of the C–N bond and a

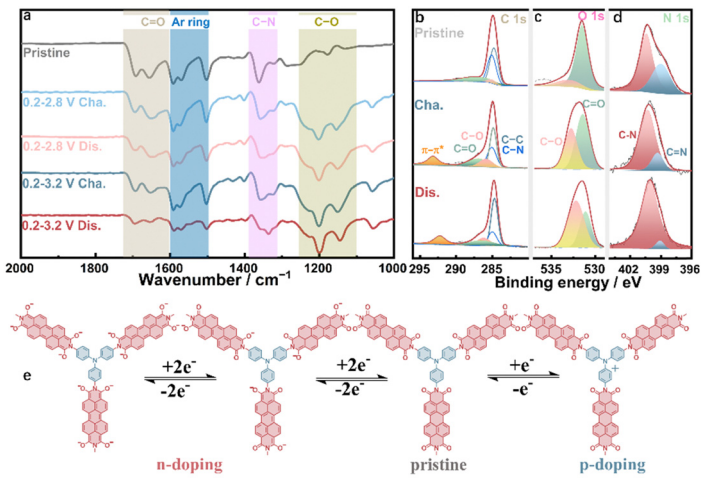

Fig. 3 (a) FT-IR spectra of **PI-P-tBA** in the pristine and charge/discharge states with the voltage ranges of 0.2–2.8 V and 0.2–3.2 V. (b) C 1s, (c) O 1s and (d) N 1s XPS spectra of **PI-P-tBA** in the pristine and charge/discharge states in the voltage range of 0.2–3.2 V. (e) Proposed redox mechanism of **PI-P-tBA**.

significant decrease in peak intensity. In addition, the change of the C–N bond peak intensity with 0.2–3.2 V is much larger than that with 0.2–2.8 V. This further demonstrates the advantages of **PI-P-tBA** as a bipolar cathode for RMBs, namely enhanced charge density changes (n- and p-doping) and electron delocalization with a large conjugated structure and wide voltage window.

The XPS results also confirm the reaction mechanism. As shown in the C 1s spectra (Fig. 3b), an obvious π–π* satellite peak appears at about 292 eV of the discharged state after a full activation, which firmly indicates the enhanced charge delocalization ability of the large conjugated **PI-P-tBA**. Different from typical enolizations, the π–π* satellite peak herein moves towards higher/lower binding energies during charge/discharge, possibly due to the positive/negative charge delocalization, respectively. Meanwhile, the C═O peak is weakened during discharge along with enhancement of the C–O peak, which is more evident in the O 1s XPS spectra (Fig. 3c). This demonstrates the reversible carbonyl enolization. In the N 1s spectra (Fig. 3d), both C–N (400.4 eV) and C═N (399 eV) peaks could be observed, which is ascribed to the conjugation of the PTCDI and tBA units. The C═N peak becomes almost negligible at discharge since electrons are delocalized to the conjugated structures. Fig. 3e shows the reaction mechanism of **PI-P-tBA** based on the above characterization. As a bipolar cathode, **PI-P-tBA** undergoes either n-doping (carbonyl enolization) upon discharge or p-doping upon charge from the pristine state. The large conjugated structure guarantees the charge delocalization and structure stability, and thus **PI-P-tBA** provides a high capacity with stable cycling.

In this study, a bipolar conjugated polymer of **PI-P-tBA** is synthesized and investigated as the cathode material of RMBs, using PTCDI and tBA units as the n- and p-type groups, respectively. The introduction of p-type unit tBA extends the conjugated structure and improves the capacity. **PI-P-tBA** exhibits a high reversible capacity of 250 mA h g^{-1} at 50 mA g^{-1} with 0.2–3.2 V, as well as good rate capability and cycling stability. The mechanism study reveals that the tBA group participated in the p-doping reactions and enhanced the n-doping activity *via* extension of the conjugated structure. The results herein provide an effective method to improve the reversible capacity and cycling stability of organic cathode materials for RMBs.

This work was financially supported by the National Natural Science Foundation of China (52172266, 22179101 and U23A20691), the Hubei Provincial Natural Science Foundation (2024AFB750), the Fundamental Research Funds for the Central Universities of South-Central Minzu University (CZD24001), and the Academic Innovation Teams of South-Central Minzu University (XTZ24012).

Data availability

The data supporting this article have been included as part of the ESI.†

Conflicts of interest

There are no conflicts to declare.

Notes and references

1 Z. Li, J. Häcker, M. Fichtner and Z. Zhao-Karger, *Adv. Energy Mater.*, 2023, **13**, 2300682.
2 D. Zhang, Y. Wang, Y. Yang, Y. Zhang, Y. Zhao, M. Pan, Y. Sun, S. Chen, X. Liu, J. Wang and Y. NuLi, *Adv. Energy Mater.*, 2023, 2301795.
3 D. Tao, T. Li, Y. Tang, H. Gui, Y. Cao and F. Xu, *ACS Nano*, 2024, **18**, 5590–5598.
4 B. Ma, C. Tan, L. Ouyang, H. Shao, N. Wang and M. Zhu, *J. Alloys Compd.*, 2022, **918**, 165803.
5 B. Ma, L. Ouyang and J. Zheng, *J. Magnes. Alloys*, 2024, **12**, 4191–4204.
6 B. Ma, W. Jiang, L. Ouyang and H. Li, *Inorg. Chem. Front.*, 2023, **10**, 6879–6891.
7 M. Mao, X. Ji, S. Hou, T. Gao, F. Wang, L. Chen, X. Fan, J. Chen, J. Ma and C. Wang, *Chem. Mater.*, 2019, **3**, 3183–3191.
8 X. Xu, F. Xiong, J. Meng, X. Wang, C. Niu, Q. An and L. Mai, *Adv. Funct. Mater.*, 2020, **30**, 1904398.
9 A. Roy, M. Sotoudeh, S. Dinda, Y. S. Tang, C. Kübel, A. Groß, Z. R. Zhao-Karger, M. Fichtner and Z. Li, *Nat. Commun.*, 2024, **15**, 492.
10 X. Ren, D. Tao, S. Cui, T. Li, Y. Cao and F. Xu, *Energy Storage Mater.*, 2023, **63**, 102992.
11 X. Song, X. Xue, H. Xia, L. Jin, A. Tao, Y. Wang, J. Liang, Y. Liu, P. Zhang, Z. Tie, Y. Long and Z. Jin, *Energy Storage Mater.*, 2023, **55**, 426–435.
12 C. Pei, F. Xiong, Y. Yin, Z. Liu, H. Tang, R. Sun, Q. An and L. Mai, *Small*, 2021, **17**, 2004108.
13 B. Pan, J. Huang, Z. Feng, L. Zeng, M. He, L. Zhang, J. T. Vaughey, M. J. Bedzyk, P. Fenter, Z. Zhang, A. K. Burrell and C. Liao, *Adv. Energy Mater.*, 2016, **6**, 1600140.
14 Y. Wang, Z. Liu, C. Wang, Y. Hu, H. Lin, W. Kong, J. Ma and Z. Jin, *Energy Storage Mater.*, 2020, **26**, 494–502.
15 S. Cui, T. Li, D. Tao, D. Zhang, Y. Cao and F. Xu, *Energy Storage Mater.*, 2024, **71**, 103672.
16 E. Zhou, X. Zhang, L. Zhu, D. Yuan and Y. Wang, *Adv. Funct. Mater.*, 2023, **33**, 2213667.
17 Z. Song, H. Zhan and Y. Zhou, *Angew. Chem., Int. Ed.*, 2010, **49**, 1–6.
18 L. Cui, L. Zhou, K. Zhang, F. Xiong, S. Tan, M. Li, Q. An, Y. Kang and L. Mai, *Nano Energy*, 2019, **65**, 103902.